Wrapping up : nidovirus membrane structures and innate immunity

Oudshoorn, D.

Chapter 4

Middle East respiratory syndrome-coronavirus nonstructural proteins 3 and 4 are required and sufficient to induce the formation of double-membrane vesicles

Diede Oudshoorn, Kevin Rijs, Ronald W.A.L. Limpens, Kevin Groen, Abraham J Koster, Eric J Snijder, Marjolein Kikkert, Montserrat Bárcena

Revised manuscript accepted for publication in mBio (mBio 8(6) e01658-17)

ABSTRACT

Betacoronaviruses such as Middle East Respiratory Syndrome-Coronavirus (MERS-CoV) are important pathogens causing potentially lethal infections in humans and animals. Coronavirus RNA synthesis is thought to be associated with replication organelles (ROs) consisting of modified endoplasmic reticulum membranes. These are transformed into double-membrane vesicles (DMVs) that contain viral double-stranded RNA, convoluted membranes, and other membranous elements, together forming a reticulovesicular network. Previous evidence suggested that the non-structural proteins (nsps) 3, 4, and 6 of the Severe Acute Respiratory Syndrome-Coronavirus (SARS-CoV), which contain transmembrane domains, are required for DMV formation. We have now expressed MERS-CoV replicase self-cleaving polyprotein fragments encompassing nsp3-4 or nsp3-6, as well as co-expressed nsp3 and nsp4 of either MERS-CoV or SARS-CoV, to characterize the membrane structures induced. Using electron tomography, we found that, for both MERS-CoV and SARS-CoV, co-expression of nsp3 and nsp4 is clearly required and sufficient to induce DMVs. DMV formation was similar when MERS-CoV nsp3 and nsp4 were co-expressed either as individual proteins or as a self-cleaving nsp3-4 precursor. Moreover, using polyprotein expression, we established that cleavage of the nsp3/nsp4 junction is essential for MERS-CoV DMV formation. Addition of the third MERS-CoV transmembrane protein, nsp6, did not seem to affect DMV formation, while its impact on the formation of other RO elements remains to be further investigated. These findings provide important insight into the formation of coronavirus ROs and establish strong similarities with RO formation by other nidoviruses, specifically the arteriviruses.

Importance

The replication of all plus-stranded RNA viruses of eukaryotes is thought to take place at cytoplasmic membranous replication organelles (ROs). One of the most prominent types of viral ROs induced by a number of these viruses, including coronaviruses, are double-membrane vesicles (DMVs) that contain viral double-stranded RNA. In this study, using electron microscopy and tomography, we explored which viral proteins are required for the formation of MERS- and SARS-coronavirus-induced DMVs. We found that co-expression of two of the three transmembrane subunits of the coronavirus replicase polyprotein, non-structural proteins (nsps) 3 and 4, is required and sufficient to induce DMV formation. In contrast to a previous report, the third transmembrane protein, nsp6, seems to be dispensable. Moreover, release of nsp3 and nsp4 from the polyprotein by proteolytic maturation is essential for DMV formation. These findings provide a strong basis for further research on the biogenesis and functionality of coronavirus ROs.

INTRODUCTION

Coronaviruses are positive-strand RNA viruses that can pose serious zoonotic threats to human health, as evidenced by the emergence of severe acute respiratory syndrome coronavirus (SARS-CoV) in 2002 (171, 172) and, more recently, the Middle East respiratory syndrome coronavirus (MERS-CoV). Since the start of the outbreak in 2012, MERS-CoV has continued to circulate in the Arabian Peninsula (12, 173), which to date has led to almost 2,000 laboratory-confirmed human infections with a lethality rate of about 35% (http://www.who.int/emergencies/mers-cov/en/). Coronaviruses, members of the order *Nidovirales*, have the largest known positive-strand RNA genomes, ranging from 26 to 33.5 kb (13, 78, 174). The 5′-proximal two-thirds of the genome contains the replicase gene that consists of two open reading frames (ORF1a and ORF1b). ORF1a translation yields polyprotein 1a (pp1a; roughly 4,000-4,500 amino acid (aa) residues long), which, following a -1 ribosomal frameshift, can be extended with the ORF1b-encoded polyprotein to yield pp1ab (6,700-7,200 aa residues in total). The pp1a and pp1ab polyproteins contain the enzymes of the RNA-synthesizing complex that drives viral genome replication and subgenomic mRNA synthesis (175). The replicase polyproteins are co- and post-translationally processed into 15 or 16 nonstructural proteins (nsps) by two or three ORF1a-encoded proteases (76, 176-179). Depending on the coronavirus, one or two papain-like proteases (PLpro) that reside in nsp3 process the part of the polyproteins upstream of nsp4. In all coronaviruses, the region downstream of nsp4 is cleaved by the 3C-like cysteine protease or main protease (M^{pro}) located in nsp5 (Fig. 1A) (76, 176-179).

Coronaviruses, like all positive-strand RNA viruses of eukaryotes, hijack intracellular membranes to form replication organelles (ROs) (16-19, 180). These generally reside in the perinuclear region of the cell and are assumed to constitute micro-environments that promote viral RNA synthesis, while possibly shielding replicative intermediates, such as double-stranded RNA, from detection by the innate immune system. The most prominent membrane structures induced after coronavirus infection are double-membrane vesicles (DMVs) (21, 22, 106, 123-128, 181), which appear to contain double-stranded RNA, a well-known marker of positive-strand RNA virus replication (21, 167). DMVs are not only formed during the replication of coronaviruses, but are also a central component of the ROs induced by numerous other plus-stranded RNA viruses such as hepatitis C virus (HCV), and enteroviruses like poliovirus and coxsackievirus (23, 56, 65). Most of our current knowledge of coronavirus ROs has been gained through electron microscopy (EM) studies of members of the genus *Betacoronavirus*, which includes SARS-CoV, MERS-CoV, and mouse hepatitis virus (MHV) (21, 106, 125-128). Electron tomography (ET) studies of SARS-CoV-infected cells showed that DMV outer membranes are often interconnected and also connected with the endoplasmic reticulum (ER) and/or with another virus-induced structure called convoluted membranes (CM) (21). Together, they form an elaborate reticulovesicular network (RVN), for which the ER probably serves as the membrane donor organelle (21).

The three main coronaviral proteins likely responsible for RO formation are the membrane-spanning nsp3, nsp4, and nsp6 subunits (Fig. 1A) (16, 182). Each of these spans

the membrane multiple times (2, 4, and 6 times, respectively) and they have 1, 2, and 3 luminal loops, respectively, with both nsp3 and nsp4 having a large luminal loop (95, 183-185). Mutagenesis studies showed that the first luminal loop of MHV nsp4 is critical for viral replication (186, 187). Furthermore, nsp4 of both MHV and SARS-CoV contains sites (2 and 1 respectively) for N-linked glycosylation in the first luminal loop of nsp4 (95, 185, 188). When both these sites were mutated in MHV nsp4 (186, 188), the virus was attenuated in cell culture and DMV formation was impaired, suggesting that nsp4 plays a critical role in coronaviral RO formation. The combined membrane-spanning regions of these proteins (i.e. including all luminal loops and flanking transmembrane domains) are commonly referred to as TM1, TM2, and TM3, respectively. Nsp3, nsp4, and nsp6 are non-conventional transmembrane proteins in the sense that they are derived from a polyprotein and do not contain N-terminal signal sequences for co-translational membrane insertion. It is currently unknown how their membrane insertion is facilitated and whether polyprotein cleavage precedes (or is required for) translocation across the ER membrane. To a certain extent, nsp2, nsp3, and nsp5 of the distantly related arteriviruses (also members of the *Nidovirales* order) can be considered equivalent to coronavirus nsp3, nsp4, and nsp6, in terms of their relative position in the replicase polyprotein and their membrane-spanning properties. For arteriviruses, expression of nsp2 and nsp3 alone was necessary and sufficient for the formation of double-membrane structures strikingly resembling the DMVs observed in infected cells (24). Co-expression of nsp5 reduced the size of the induced DMVs, but did not change their overall architecture (180). In the case of coronaviruses, it was recently reported that the transient co-expression of SARS-CoV nsp3, nsp4, and nsp6 led to the formation of DMVs (28). Cells co-expressing nsp3 and nsp4 alone contained so-called maze-like bodies, consisting of paired ER membranes (zippered ER) and some circular profiles that were interpreted as cross-sections of double-membrane tubules. Therefore, it was concluded that nsp6 is essential for the biogenesis of SARS-CoV DMVs, whereas nsp3 and nsp4 can mediate the pairing of membranes that are likely an intermediate in DMV formation (28).

In the current study, we examined the role of MERS-CoV nsps in betacoronavirus RO biogenesis. Using EM and ET, we found that MERS-CoV nsp3 and nsp4, either co-expressed from separate plasmids or expressed as a self-cleaving polyprotein fragment (nsp3-4), are essential and sufficient for the formation of DMVs that assemble into an RVN. Addition of the third transmembrane subunit of the MERS-CoV replicase, nsp6, did not alter the overall morphology of the induced DMVs. When the nsp3-4 polyprotein remained uncleaved, this prevented the formation of DMVs while membrane pairing did still occur, suggesting that proteolytic processing coordinates DMV formation in time and/or space. To compare our results with previous work, we used ET to analyze the 3D structure of the maze-like bodies induced upon co-expression of SARS-CoV nsp3 and nsp4, and established that also in the case of SARS-CoV these proteins suffice for DMV formation. Our results provide important new insights in the biogenesis of coronavirus ROs and suggest the conservation of certain principles underlying RO formation among distantly related members of the order *Nidovirales*.

RESULTS

MERS-CoV nsp3 and nsp4 co-localize in the perinuclear region of the cell

To study whether the transmembrane nsps of MERS-CoV are able to induce DMV formation, we expressed nsp3 and nsp4 from a CAG promoter (189) either by co-transfection of cells with plasmids encoding individual proteins or by transfection with a single plasmid encoding a self-cleaving nsp3-4 polyprotein fragment (Fig. 1A). Constructs were codon-optimized for expression in human cells, (potential) splice sites were eliminated, and the encoded proteins were equipped with HA, myc, or V5 tags at their termini. The constructs were transfected into 293T cells to verify protein expression and processing (Fig. 1B). The wild-type nsp3-4 polyprotein was fully cleaved into mature nsp3 and nsp4, as was previously described (190). As a control, a mutant in which the nsp3/nsp4 cleavage site was inactivated (G2739A/G2740A; GG>AA; (191)) was included to generate the non-cleaved precursor. Interactions between nsp3 and nsp4 were previously shown to occur for MHV and SARS-CoV (161, 162) and we assessed whether this was also the case for the corresponding MERS-CoV proteins. To this end, 293T cells were transfected with a construct expressing HA-nsp3-myc or nsp4-V5, or co-transfected with both constructs. Expression products were labeled metabolically with [^{35}S]methionine and [^{35}S]cysteine, and subsequently immunoprecipitated with either HA- or V5-specific antibodies (Fig. 1C). Upon immunoprecipitation with the HA-specific antiserum, nsp4-V5 was brought down when HA-nsp3 was present (left panel). Conversely, when using the V5-specific antibody, HA-nsp3 was co-immunoprecipitated when nsp4-V5 was present (right panel). These findings demonstrated that these two MERS-CoV proteins interact and further supported the notion that this is a common feature of coronaviruses. When using immunofluorescence microscopy, separate expression of nsp3 or nsp4 in HuH-7 cells yielded a reticular labeling pattern, with some more intense foci in the perinuclear region of the cell, suggesting that – in the absence of the other – either protein localized at least partially to the ER (Fig. 1D). This reticular pattern (but without the foci) has been described previously upon transient expression of MHV and SARS-CoV nsp4 (95, 96), whereas full-length SARS-CoV nsp3 was reported to localize to foci similar to those we observed (28). When co-expressing MERS-CoV nsp3 and nsp4, or when expressing the self-cleaving nsp3-4 polyprotein, the reticular pattern was much less pronounced and both proteins mainly co-localized in foci in the perinuclear region (Fig. 1D lower panels). This was in agreement with the finding that MERS-CoV nsp3 and nsp4 interact and also suggested that this interaction strongly promotes their recruitment to the foci in the perinuclear region. However, the resolution of light microscopy does not allow drawing conclusions about the ultrastructure of the subcellular structures in which these proteins accumulate.

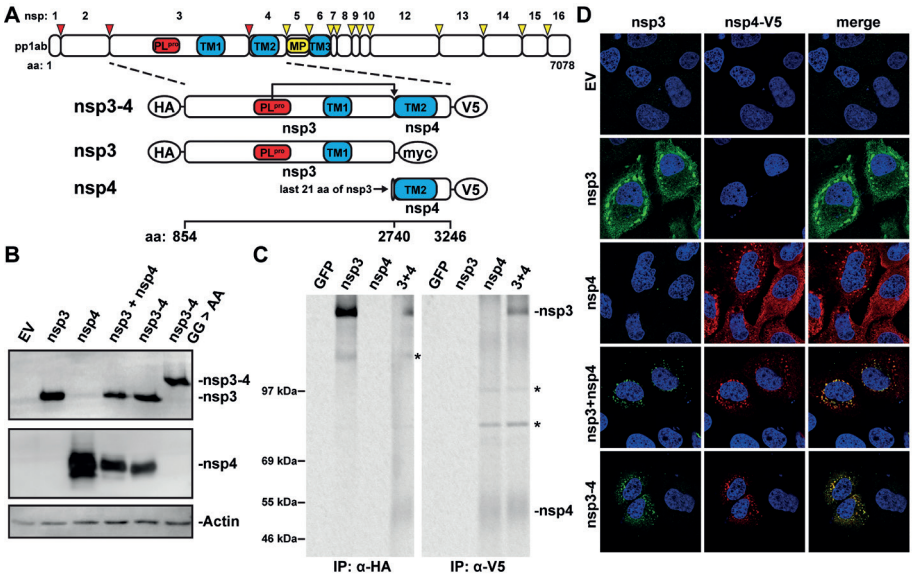

Fig. 1. MERS-CoV nsp3 and nsp4 interact with each other. (A) *Scaled schematic overview of MERS-CoV pp1ab and nsp3-4 constructs. Amino acid numbers refer to the MERS-CoV pp1ab sequence. The expected cleavage of nsp3/nsp4 junction by PL^{pro} is indicated. The epitope tags used at the termini of the constructs are indicated with ovals. TM = transmembrane region.* **(B)** *293T cells were transfected with MERS-CoV nsp3-4 plasmids or empty pCAGGS vector (EV) and analyzed by Western blotting 20 hours post transfection. Nsp3 was detected with α-SARS-CoV nsp3 serum that cross-reacts with MERS-CoV nsp3 (128) and nsp4 was detected with α-V5 monoclonal antibody.* **(C)** *Constructs expressing MERS-CoV nsp3, nsp4 or a GFP control were transfected into 293T cells, which were metabolically labeled with [^{35}S] methionine/cysteine from 4 to 20 hours post transfection. Lysates were immunoprecipitated with the indicated antibodies, separated on a SDS-PAGE gel and visualized using phosphor imaging. Bands not corresponding to expected protein size in Western Blot were indicated with asterisks. The ± 130kDa band in the nsp3 IP was also observed in Western Blot. Nsp4 bands in IP were fuzzy likely due to the relatively high hydrophobicity of the protein.* **(D)** *HuH-7 cells were transfected with the indicated plasmids and localization of MERS-CoV nsp3 and nsp4 was analyzed using immunofluorescence labeling and confocal microscopy at 24 hours post transfection. Nsp3 was detected with α-SARS-CoV-nsp3 serum and nsp4 with α-V5 monoclonal antibody.*

MERS-CoV nsp3 and nsp4 are required and sufficient to induce DMV formation

The next step was to determine whether nsp3 and nsp4 could induce the formation of double-membrane structures similar to those observed during infection. As a reference, MERS-CoV-infected HuH-7 cells were analyzed by EM. The membrane structures that were previously described in high-pressure frozen and freeze-substituted Vero cells infected with MERS-CoV (128) were readily apparent at 10 h post infection (p.i.) in chemically fixed HuH-7 cells (Fig. 2A). Numerous DMVs were found (red asterisks), often adjacent to areas containing CM. The DMV interior appeared electron-translucent, a difference with cryo-

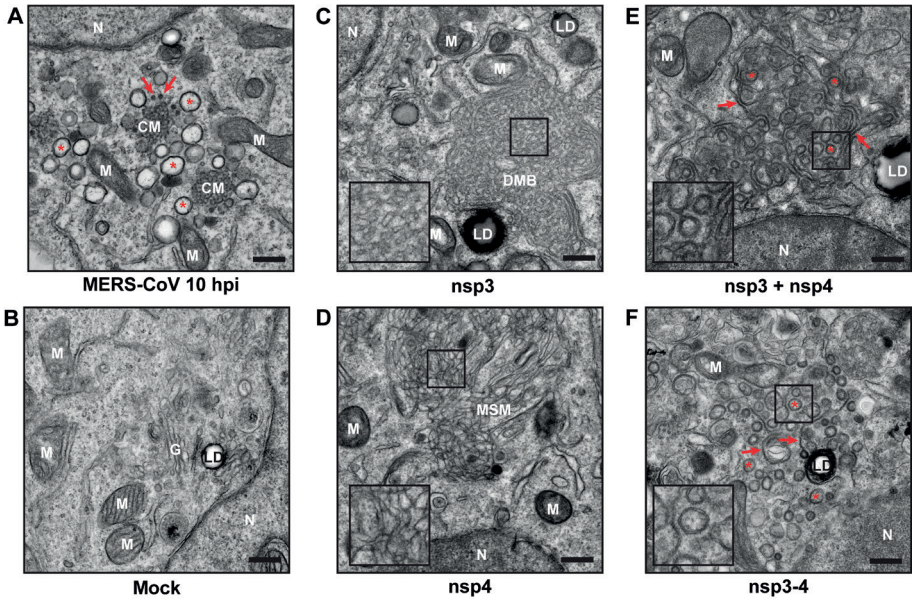

Fig. 2. MERS-CoV nsp3 and nsp4 induce modification of intracellular membranes. (A) *HuH-7 cells were infected with MERS-CoV or mock infected* **(B)** *and analyzed at 10 h p.i. using EM. Several DMVs are indicated with red asterisks and several spherules are indicated with red arrows.* **(C-F)** *HuH-7 cells were transfected either with constructs expressing individual nsps (C,D) or both nsp3 and nsp4, following either co-transfection with two plasmids (nsp3 + nsp4) or expression of a self-cleaving precursor (nsp3-4) (E/F), and analyzed using EM at 24 hours post transfection. (E,F) Some stretches of zippered-ER are indicated with red arrows and several DMVs are indicated with red asterisks. (A-F) N = nucleus; G = Golgi; M = mitochondria; LD = lipid droplet; CM = convoluted membranes; DMB = disordered-membrane body; MSM = clusters of modified single-membranes; all scale bars represent 500 nm.*

fixed samples (128) that can likely be attributed to the different sample preparation method as the contents of SARS-CoV induced DMVs are easily lost upon chemical fixation (106). Occasionally some small(er) circular structures were observed that seemed similar in size to the spherules recently described for the gammacoronavirus infectious bronchitis virus (red arrows) (22). None of these structures were found in mock-infected control samples (Fig. 2B).

When HuH-7 cells expressed either nsp3 or nsp4, areas containing modified membranes were observed, which likely corresponded to the foci observed in fluorescence microscopy (Fig. 1D). In nsp3-expressing cells (Fig. 2C), we detected large regions, usually several microns in diameter, of disordered membrane bodies (DMB), which were similar to those previously observed after SARS-CoV nsp3 expression (28). The membrane structures clustering in these DMBs were reminiscent of the surrounding ER cisternae, with which they were frequently connected, suggesting that DMBs consisted of clustered ER-derived membranes. Upon expression of MERS-CoV nsp4, large clusters of modified single membranes (MSM) were observed (Fig. 2D), but these structures seemed more

irregular when compared to those induced by nsp3 (Fig. 2C). The expression of SARS-CoV nsp4 did not result in changes in intracellular membrane morphology (28), in contrast with our present observations following MERS-CoV nsp4 expression. Whether this reflects differences between the experimental setups used or an actual difference between these viral proteins remains to be determined.

When MERS-CoV nsp3 and nsp4 were expressed in the same cell, either by co-transfection or by expression of the self-cleaving nsp3-4 polyprotein, a remarkably different set of membrane structures was observed (Fig. 2E,F). A combination of circular double-membrane profiles (red asterisks) and paired membranes (red arrows) was present in both cases, suggesting that the combined expression of MERS-CoV nsp3 and nsp4 is sufficient to induce DMV formation. There was no apparent difference between the structures resulting from co-expression of nsp3 and nsp4 versus expression of the self-cleaving nsp3-4 polyprotein (Fig. 2E,F), but in both cases the circular profiles were significantly smaller than the ones observed in MERS-CoV infected cells (average diameters 146 and 148 nm, respectively, versus 252 nm in infection) (Sup Fig. 1).

To verify that DMVs are indeed formed upon expression of nsp3 + nsp4 and nsp3-4, we analyzed the 3D architecture of these membrane structures using ET, which confirmed that multiple circular profiles indeed corresponded to DMVs (Supplementary movies 3 and 4, Fig. 3A). We found no openings connecting the DMV interior and the cytosol, similar to what was observed previously in tomographic analysis of coronavirus-infected cells (21, 22). The tomograms corroborated the structural similarity between the membrane structures induced by co-transfection with nsp3 and nsp4 constructs and by expression of the nsp3-4 polyprotein. The electron density of the DMV interior seemed similar to that of the surrounding cytoplasm and in this sense it was different from the DMVs observed in MERS-CoV infected cells (compare to Fig. 3A), which is likely due to the absence of other viral proteins and double-stranded RNA. In some cases, DMVs appeared to be contained in a larger double-membrane structure (Fig. 3B; red asterisks). Such structures have not been observed in coronavirus-infected cells so far and their formation could be linked to *e.g.* the absence of (viral) DMV content or levels of the nsp3 and nsp4 proteins. The paired membranes were often continuous with the ER (Fig. 3B) and resembled the so-called zippered ER that has been also observed in IBV-infected cells (22), although they have not been documented so far for betacoronavirus-infected cells. These paired membranes may represent an intermediate of DMV biogenesis. Further supporting this explanation, structures in which the zippered ER seemed to transform into a nascent DMV could be observed in the tomograms (Fig. 3B; red arrows). We also observed DMV-DMV, DMV-zippered ER, and DMV-ER connections (Fig. 3C; red arrows), and completely isolated DMVs were in fact rare. Together, these observations suggest that MERS-CoV nsp3 and nsp4 are capable of inducing the transformation of ER membranes into an RVN of modified ER and DMVs.

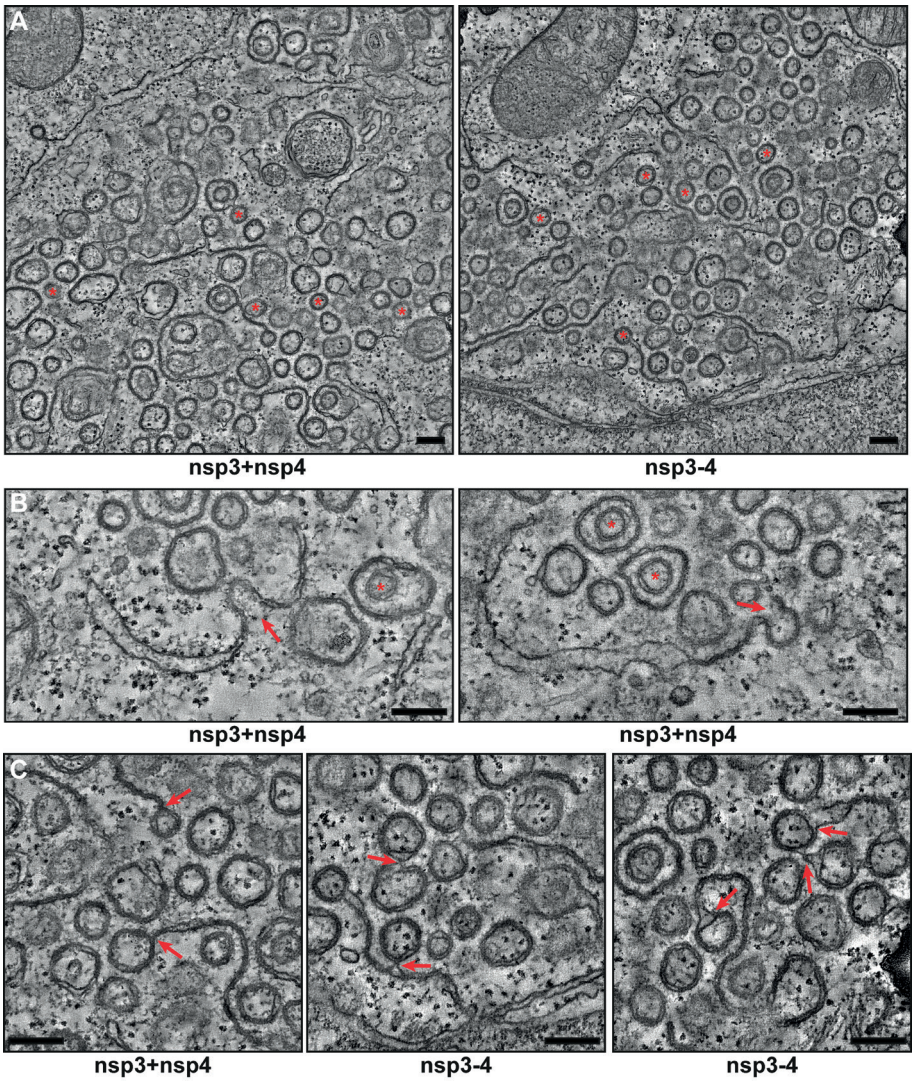

Fig. 3. MERS-CoV nsp3 and nsp4 induce the formation of DMVs that are organized in an RVN. *HuH-7 cells were co-transfected with constructs expressing nsp3 and nsp4 or the nsp3-4 precursor and fixed for ET analysis.* **(A)** *Overviews of reconstructed tomograms (available as supplementary movies S1 and S2, respectively) for both conditions. Some of the fully reconstructed closed DMVs are indicated with red asterisks.* **(B)** *Zippered-ER curving into putative intermediates during DMV biogenesis (indicated with red arrows) is shown. Two DMVs that are enclosed within other DMVs are indicated with red asterisks.* **(C)** *Examples of connections between DMVs and (zippered) ER (indicated with red arrows). All the images are virtual 5 nm thick slices from the reconstructed tomograms. All scale bars represent 250 nm.*

MERS-CoV nsp6 does not alter DMV morphology

The DMVs induced by expression of MERS-CoV nsp3-4 largely mimicked those observed during infection. However, the additional RVN elements that have been observed in this and previous studies of coronavirus-infected cells (CM and spherules) were not detected. To investigate whether nsp6, the third transmembrane subunit of the coronavirus replicase, plays a role in their formation or affects DMV formation, we extended the expressed polyprotein fragment to include nsp5 and nsp6. In addition to PLpro cleaving the nsp3/nsp4 site in this polyprotein fragment, the nsp5-based M^{pro} was expected to perform the cleavages at the nsp4/nsp5 and nsp5/nsp6 junctions. It should be noted, however, that the kinetics of polyprotein cleavage during MERS-CoV infection have not been documented; for example, it is unknown whether specific intermediates of polyprotein cleavage are long-lived and/or perform specific functions during MERS-CoV replication. Unfortunately, our efforts to investigate this matter in MERS-CoV-infected cells were hampered by technical difficulties arising from the insufficient levels of 35S-labelled pp1a/pp1ab subunits for immunoprecipitation analysis.

We therefore designed several polyprotein constructs encompassing the nsp3-6 region of MERS-CoV pp1a and tested their proteolytic processing as part of our evaluation of the impact of nsp6 expression on the formation of the coronavirus ROs (Fig. 4A). Upon expression of an HA-nsp3-6-V5 polyprotein and labeling with [^{35}S]methionine/cysteine, immunoprecipitation analysis showed that only a trace amount of fully cleaved nsp4 and nsp5 was present (Fig. 4B; lanes 3 and 8) and that most of the signal was present in larger precursors. Given the interaction between nsp3 and nsp4 (Fig. 1C) and the fact that the nsp5-6 precursor did not co-immunoprecipitate with the HA-tagged nsp3 (lane 3), we assumed the second, larger band to be co-precipitating nsp4-6 precursor. When a rabbit antiserum raised against a combination of MERS-CoV nsp5 peptides was used (lane 8), two precursors were pulled down. The smallest of these co-migrated with the nsp5-6 precursor (lane 13), which was expressed from an nsp5-6 construct carrying an nsp5/nsp6 cleavage site mutation (Q3553A). Based on its migration in the gel, a possible dimer of the nsp5-6 precursor was also observed, which co-migrated with nsp4-6 observed in lanes 3 and 8.

As in the nsp3- and nsp4-coding sequences used above, the codon usage of the nsp5 and nsp6 genes in our constructs was optimized for expression in human cells. One caveat is that this approach may eliminate rare codons that can reduce ribosome processivity during translation to promote proper protein folding, which can be particularly important for transmembrane proteins (192). Nsp6 is the coronavirus transmembrane nsp with the largest number of predicted membrane-spanning domains and its folding and proper membrane insertion might be linked to polyprotein processing. We therefore swapped the codon-optimized nsp6 gene for the original viral sequence. Furthermore, anticipating that the C-terminal V5-tag could be an issue, we restored the nsp6/7 cleavage site to yield the native nsp6 C-terminus after cleavage. Downstream of the short nsp7 peptide, GFP was fused to the C-terminus of the polyprotein so that its cleavage could be monitored (Fig. 4A; nsp3-6-GFP). This approach, however, only marginally improved the processing by M^{pro} as only small amounts of free nsp4, nsp5, and GFP were observed and most of the signal

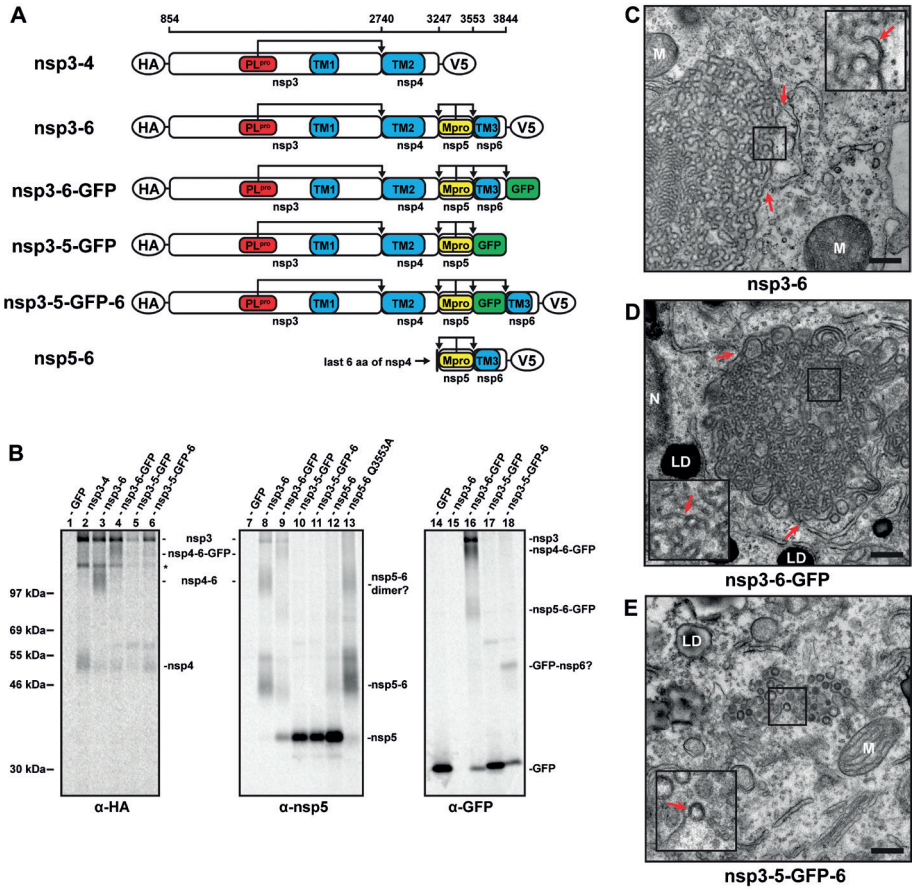

Fig. 4. Co-expression of MERS-CoV nsp6 does not alter DMV morphology. (A) *Scaled schematic overview of MERS-CoV nsp3-6 constructs. Amino acid numbers at the top are the positions in MERS-CoV pp1a. Expected cleavage sites by PL^{pro} and M^{pro} are indicated. TM = transmembrane domain, used epitope tags are indicated with ovals.* **(B)** *293T cells were transfected with indicated plasmids and metabolically labeled with [^{35}S]methionine/cysteine from 4 to 20 hours post transfection. Lysates were immunoprecipitated with indicated antibodies and separated on a SDS-PAGE gel. The ~130 kDa band in the nsp3 sample (indicated with an asterisk) is the same as in (Fig. 1C) and was also observed when only nsp3 was expressed. Nsp4 bands and putative nsp4- and nsp6-containing precursor bands were fuzzy, likely due to their relatively large hydrophobic domains. The different GFP bands around 30 kDa vary in size due to small variations in the length of the linker in the different polyprotein constructs.* **(C,D,E)** *HuH-7 cells were transfected with indicated plasmids and analyzed using EM at 24 hours post transfection. Red arrows indicate possible connections between the ER and the cubic membranes and some DMVs are indicated with red asterisks. The insets show some areas where the double membrane can be observed. N = nucleus; M = mitochondria; LD = lipid droplet; all scale bars represent 500 nm.*

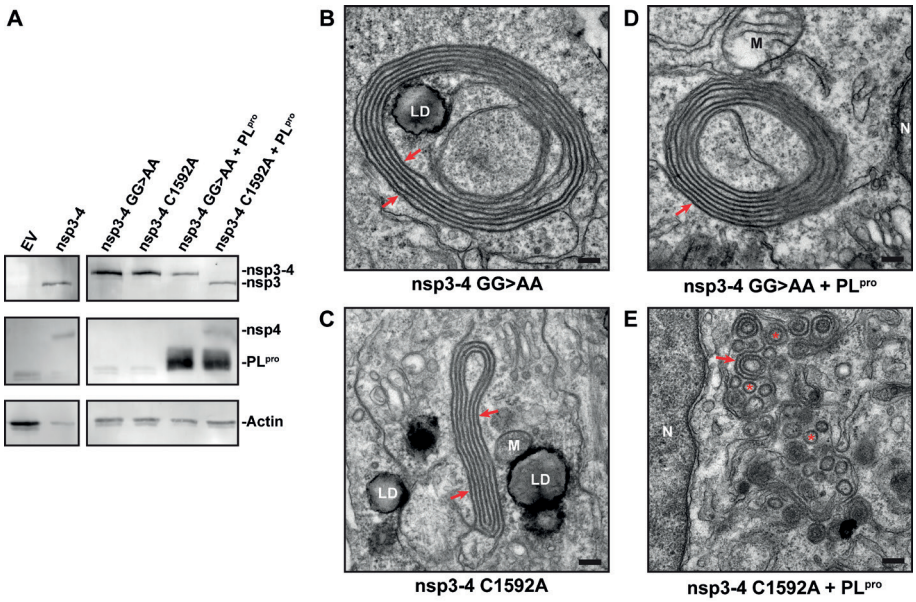

Fig. 5. Cleavage of MERS-CoV nsp3/nsp4 junction is essential for DMV formation. (A) *293T cells were transfected with indicated plasmids and analyzed using Western blotting. Nsp3 was detected with α-SARS-nsp3 serum and nsp4 with α-V5 monoclonal antibody.* **(B-E)** *HuH-7 cells were transfected with mutant nsp3-4 constructs individually (B/C) or co-transfected with the PL^{pro} domain of nsp3 (D/E) and analyzed using EM. Red arrows point at zippered-ER and in panel (E) some putative DMVs are indicated with red asterisks. N = nucleus; M = mitochondria; LD = lipid droplet; all scale bars represent 500 nm.*

was still present in the form of larger precursor proteins (Fig. 4B; lanes 9 and 16). We next checked whether M^{pro} was able to fully process the nsp4/nsp5 and nsp5/nsp6 junctions in other polyprotein configurations. To this end we used an nsp3-5-GFP polyprotein of which the nsp5/nsp6 junction was intact but followed, after a short nsp6 linker, by the GFP sequence (Fig. 4A; nsp3-5-GFP), and an nsp5-6 polyprotein carrying a small C-terminal nsp4 peptide at its N-terminus (Fig. 4A; nsp5-6). For both of these polyproteins, we observed near-complete proteolytic processing (Fig. 4B; lanes 10, 12, and 17), which suggested that in the case of nsp3-6-GFP the simultaneous expression of nsp4 and nsp6 impaired the kinetics of polyprotein processing. In an attempt to trigger efficient proteolytic processing of a polyprotein containing all three MERS-CoV transmembrane nsps, we duplicated the nsp5/nsp6 junction and inserted GFP between the two copies (Fig. 4A; nsp3-5-GFP-6). This polyprotein was processed reasonably efficiently, as mature nsp5 and a substantial amount of free GFP were observed, although some of the remaining signal may have corresponded to uncleaved GFP-nsp6 (Fig. 4B; lanes 11 and 18). Even though several questions remained regarding the identity of some of the larger cleavage products and the kinetics of polyprotein processing, the different MERS-CoV nsp3-6 constructs offered a useful tool to evaluate the effect of expressing nsp6 in addition to nsp3 and nsp4.

When the inefficiently processed nsp3-6 precursor was expressed in HuH-7 cells, we no longer found DMVs, but instead large areas of highly organized and curved membrane structures were seen (Fig. 4C). Similar structures were observed when the nsp3-6-GFP polyprotein was expressed (Fig. 4D). In both cases, the structures were connected to surrounding ER cisternae (Fig. 4C,D; red arrows) and, in contrast to the large single-membrane clusters observed in nsp3- or nsp4-expressing cells (Fig. 2C,D), they consisted of double membranes (Fig. 4C,D; red arrows in insets). The geometrical pattern in these large areas containing double-membrane structures is typical of cubic membranes (193). Possible triggers of cubic membrane formation are over-expression and/or misfolding of ER proteins, which can lead to protein and membrane aggregation, which possibly happened here. When we instead expressed the nsp3-5-GFP-6 polyprotein, which was almost fully processed (see above), rather than cubic membranes we observed putative DMVs together with zippered-ER (Fig. 4E). These membrane structures were very similar to the ones found in cells expressing just nsp3 and nsp4 (compare with Fig. 2E,F). The average size of these DMVs (146 nm) was very similar to that of DMVs induced by nsp3-4 expression (148 nm) (Sup Fig. 1). The circular profiles (putative DMVs) were detected in 33 out of 642 cell profiles analyzed; however, none of these regions contained CM or spherules. This suggests that, while nsp3 and nsp4 are necessary and sufficient for the rearrangement of intracellular membranes into DMVs, the presence of (cleaved) nsp6 does not suffice to trigger the formation of the additional membrane structures typical of MERS-CoV infection. Other viral components that are present during MERS-CoV replication, such as viral RNA or other viral proteins, might thus be required for the formation of convoluted membranes and spherules.

Cleavage of the MERS-CoV nsp3/nsp4 junction is essential for DMV formation

To gain more insight in the biogenesis of coronavirus DMVs, we set out to determine the role of the nsp3/nsp4 cleavage event. We surmised that the membrane modifications induced by an uncleaved nsp3-4 polyprotein could differ from those triggered by the (cleaved or co-expressed) nsp3 and nsp4 subunits. We transfected HuH-7 cells with plasmids encoding nsp3-4 carrying either a mutated nsp3/nsp4 cleavage site (GG>AA) or a catalytic site mutation in the nsp3 PL^{pro} domain (C1592A) that inactivates the protease (194). In both cases, only the uncleaved nsp3-4 precursor was observed (Fig. 5A). Interestingly, DMVs were no longer found and instead we detected concentric structures consisting of zippered ER that mostly lacked the pronounced curvature present in DMVs (Fig. 5B,C). Co-transfection of the cells with a plasmid encoding the active PL^{pro} domain restored the nsp3/nsp4 cleavage in the nsp3-4 C1592A mutant polyprotein, but not in the nsp3-4 polyprotein with the mutated cleavage site (Fig. 5A). Accordingly, expression of PLpro together with the nsp3-4 cleavage site mutant (Fig. 5D) did not alter the structures observed. In contrast, when trans-cleavage of the nsp3/nsp4 site, by co-expression of PLpro with the nsp3-4 C1592A polyprotein, was achieved, DMV formation was at least partially restored and resulted in a mixture of abundant DMV and zippered ER profiles (Fig. 5E), as observed before (Fig. 2E,F). Expression of PL^{pro} by itself did not have a membrane-remodeling effect. These results clearly showed

that the nsp3-4 precursor is able to induce the membrane pairing required to form zippered ER, but that cleavage of the nsp3/nsp4 junction is essential for the formation of DMVs.

SARS-CoV nsp3 and nsp4 are also sufficient to induce DMV formation

Recently it was reported that SARS-CoV nsp3, nsp4, and nsp6 are all required for the formation of DMVs when transiently expressed as individual subunits (28). In that study, co-expression of SARS-CoV nsp3 and nsp4, but not nsp6, led to the formation of so-called maze-like bodies (MLBs), large clusters of double-membrane structures that were interpreted as closely packed double-membrane tubules. In view of our data presented above (Fig. 2E,F), this suggested that the nsp3 and nsp4 subunits of MERS-CoV and SARS-CoV differ in their ability of to induce DMV formation. These observations could reflect fundamental differences in the biogenesis of the ROs of these two betacoronaviruses or, alternatively, could result from differences in the respective experimental setups used. Such technical differences could include the transfection method (lipofection in the SARS-CoV study versus electroporation in our MERS-CoV study) and the cell type used for the EM analysis (293T cells versus HuH-7 cells, respectively). Therefore, we co-expressed nsp3 and nsp4 of either virus in 293T cells transfected using lipofection. For MERS-CoV, co-expression of nsp3 and nsp4 led to the formation of numerous circular double-membrane profiles together with some zippered ER (Fig. 6A,B), which strongly resembled what we observed in HuH-7 cells. Co-expression of SARS-CoV nsp3 and nsp4 led to the formation of MLBs very similar to those observed previously (28) with areas of zippered ER, often clustered as regularly spaced profiles, and circular double-membrane profiles (Fig. 6C,D). Angelini *et al.* (28) previously postulated that these circular profiles likely were cross sections of double-walled tubules, of which the regularly spaced zippered ER profiles would then represent longitudinal sections. The fact that the spacing between clustered zippered ER profiles roughly coincided with the diameter of the circular profiles supported this interpretation. However, the authors also admitted that ET would be required to confirm their model. To determine whether the circular profiles in the MLBs represented tubular or vesicular structures, we now used ET to analyze several MLBs, two of which are shown in Fig. 6. In one of those images, zippered ER is the dominant structure (Supplementary movies 5; Fig. 6C) whereas the other mainly contained circular double-membrane profiles (Supplementary movie 6; Fig. 6D). In both tomograms, we could detect multiple double-membrane profiles that increase and decrease in diameter when progressing through the tomogram (indicated with green dots in the tomogram movie) and ultimately disappear, indicating that they represent vesicles rather than tubules. In fact, no tubular structures were observed in the tomograms. The presumed longitudinal views of tubular structures turned out to consist of zippered-ER winding through the MLB. Our results show that, also in the case of SARS-CoV, co-expression of nsp3 and nsp4 suffices for the induction of DMV formation and strongly suggests that this is a common feature among betacoronaviruses.

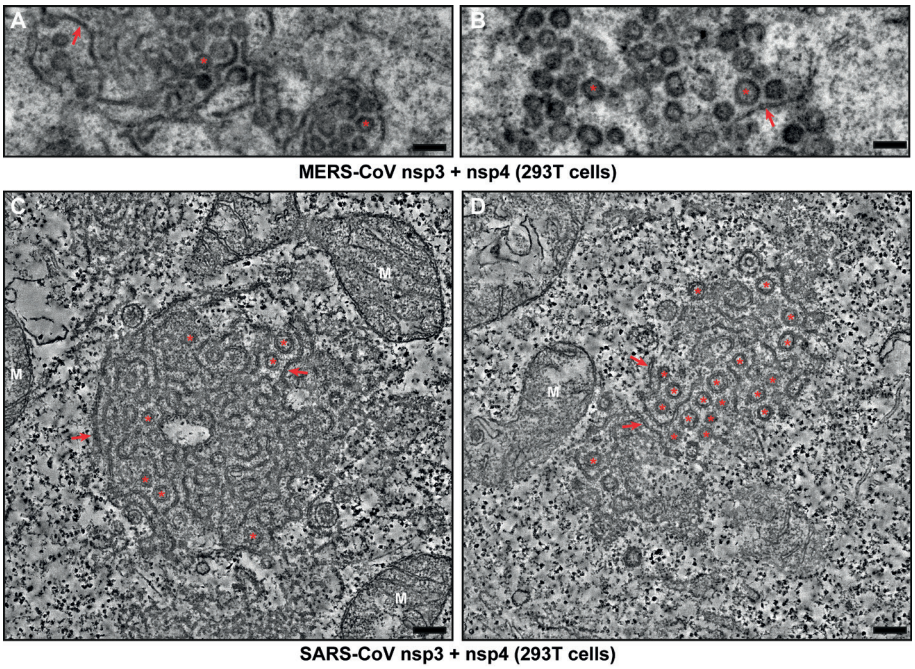

Fig. 6. SARS-CoV nsp3 and nsp4 also suffice to induce DMV formation. (A,B) *293T cells were co-transfected with plasmids encoding MERS-CoV nsp3 and nsp4 and fixed for conventional EM analysis 24 hours post-transfection. DMVs are indicated with red asterisks and red arrows point at zippered ER.* **(C,D)** *293T cells were co-transfected with plasmids encoding SARS-CoV nsp3 and nsp4 and fixed for ET analysis 24 hours post-transfection. Two virtual slices (8.5 nm) from reconstructed tomograms (available as supplementary movies S3 and S4 respectively) are shown. Red arrows indicate zippered-ER and red asterisks indicate all the DMVs that were fully reconstructed in the tomogram present in this virtual slice. All scale bars represent 250 nm.*

DISCUSSION

The generation of membranous organelles that support their replication machinery is a universal mechanism among positive-strand RNA viruses infecting eukaryotes. The formation of these ROs is induced by viral proteins (23, 25, 27), and appears to be also reliant on host factors, some of which have been identified as important players (41, 195). In this study, we sought to identify the viral proteins required to induce the formation of (beta)coronavirus DMVs, the most prominent membrane structure formed during coronavirus infection. Using ET, we found that co-expression of nsp3 and nsp4 of either SARS-CoV or MERS-CoV was required and sufficient to trigger the formation of ER-derived DMVs. Moreover, their 3D architecture was similar to what has been observed during betacoronavirus infection (21). The DMVs formed upon co-expression of nsp3 and nsp4 were closed, with no detectable opening connecting the DMV interior and the surrounding cytosol, whereas their outer membrane usually was continuous with those of other DMVs

and/or with (modified) ER. Our data importantly modify the conclusions of an earlier SARS-CoV study (28), which was based on the transient co-expression of SARS-CoV nsp3 and nsp4 from separate plasmids and the 2D imaging of the resulting membrane structures. The observation of maze-like bodies and circular double-membrane profiles, which were interpreted to probably represent tubular structures, led these authors to conclude that co-expression of SARS-CoV nsp3 and nsp4 was not sufficient for DMV formation. Using ET (Fig. 6), we could now show that the circular profiles observed in these maze-like bodies are in fact DMVs, suggesting that the basic capability of nsp3 and nsp4 to induce DMV formation probably is a common feature of betacoronaviruses. These findings also highlight the importance of 3D analysis as a tool to fully characterize the ultrastructure of membranous viral ROs.

Interestingly, in the case of the arterivirus EAV, nsp2 and nsp3 were found to be required and sufficient for DMV formation (24, 180). At least to a certain extent, these proteins can be considered the functional equivalents of coronavirus nsp3 and nsp4, respectively as they share a number of features like the presence of multiple membrane-spanning domains and a papain-like protease in the upstream protein that cleaves the junction between the two subunits. They also occupy comparable positions in the replicase polyproteins, suggesting there may also be similarities in terms of the relative order in which these subunits are synthesized, released, and targeted to the membranes they transform (16). These functional similarities and the potential to trigger DMV formation may thus be shared by these proteins of all corona- and arteriviruses, and possibly extends to other branches of the order *Nidovirales*, like the poorly studied ronivirus and mesonivirus families.

Our findings also shed more light on DMV biogenesis, for which two models have been proposed that are not mutually exclusive. The first has been termed “double budding”, where a vesicle would first bud into the ER lumen and then bud out again to acquire a second membrane. The alternative model is based on “enwrapping”: membranes would first pair or “zipper”, then curve and finally form a closed DMV after a membrane fission event (88, 180). The frequent observation of zippered ER after co-expression of nsp3 and nsp4, and multiple EM images in which zippered ER seemed to wrap into a DMV (e.g. Fig. 3B), suggest that this structure is a DMV precursor. Interestingly, whereas the uncleaved nsp3-4 precursor was able to induce the pairing of ER membranes, DMV formation only occurred upon cleavage of the nsp3/nsp4 junction, which strongly suggests that membrane pairing is an early step in DMV formation. Our findings contrast with what was observed previously for arteriviruses where cleavage of the nsp2/3 junction was not required for the formation of DMVs in an expression system (89). Together our observations favor the enwrapping model for DMV formation and, even though the existence in parallel of a double budding mechanism cannot be formally ruled out, the current data adds to the mounting evidence pointing towards double-membrane enwrapping as the central mechanism for DMV formation. For the distantly related arteriviruses (180, 196) and the unrelated picornaviruses (56, 65), putative enwrapping intermediates have been described, indicating that this might be a common mechanism of DMV-biogenesis among +RNA viruses.

Several steps are required for DMV biogenesis: pairing of membranes, membrane curvature (both positive and negative), and fission (88, 180). In the enwrapping model for DMV biogenesis membrane pairing is an early step that may be mediated directly by interactions between the viral proteins inducing DMV formation. The interaction(s) between nsp3 and nsp4 that we described here for MERS-CoV may be sufficient to facilitate membrane pairing. Similar observations have been made for SARS-CoV and MHV (28, 96). The most likely candidate regions for this kind of interactions are the luminal loops of nsp3 and nsp4 (182, 183) that are located in the TM1 and TM2 regions respectively, as these could interact with their counterparts on the opposite side of the ER cisterna, thus inducing membrane pairing. This view is partly supported by a study on MHV for which a truncated nsp3 lacking the region upstream of TM1 co-expressed with nsp4 was sufficient to induce membrane pairing but not the formation of DMVs (96). This suggests that, although the cytosolic N-terminal region of nsp3 is required for complete DMV formation, the TM1 region (together with nsp4) may be sufficient to induce membrane pairing. In addition, the liberation (by PL^{pro}-mediated cleavage of the nsp3/nsp4 junction) and presumed membrane insertion of the hydrophobic N-terminal domain of nsp4 may be an important determinant of the ultimate trans-membrane configuration of this protein, potentially with direct implications for the transformation of zippered ER into DMVs. However, we found no major differences between DMVs induced by expression of self-cleaving MERS-CoV nsp3-4 compared to co-expression of nsp3 and nsp4, suggesting that nsp4 is properly inserted in the membrane when individually expressed. The concentric zippered ER observed after expression of the uncleaved nsp3-4 polyprotein could then reflect an intermediate stage in which the lack of nsp3/nsp4 cleavage prevents proper membrane remodeling. The proximal (and largest) luminal loop of nsp4 contains a N-linked glycosylation site (N2985 in MERS-CoV), similar to the glycosylation site(s) in SARS-CoV and MHV (95, 185, 188). Analysis of the use of that site in proteolytically processed nsp4 and the uncleaved nsp3-4 precursor could provide insight in the sequence of events leading to the membrane insertion of MERS-CoV nsp4.

Although our data establish that expression of nsp3 and nsp4 suffices for coronaviral DMV formation, the precise role in this process – if any – of the nsp6 transmembrane subunit remains unclear. Our current data suggest that, compared to cells expressing MERS-CoV nsp3 and nsp4 only, co-expression of cleaved nsp6 does not affect DMV formation, nor does it lead to the formation of additional structures like CM or spherules. However, co-expression of SARS-CoV nsp3, nsp4, and nsp6 was previously shown to induce CM formation (in addition to DMVs) (28). When MERS-CoV nsp6 was retained in an unprocessed nsp4-6 precursor (Fig. 4B), DMVs were no longer formed and membrane clusters appeared that resemble cubic membranes. It has been proposed that the CM formed by coronaviruses are in fact a form of cubic membranes (197). This might be related to observations that, compared to DMVs, CM are mostly formed relatively late in infection (21, 127) when (viral) proteins or polyprotein fragments accumulate. It is conceivable that such accumulation could lead to aggregation, misfolding, and/or impaired polyprotein processing resulting in the formation of cubic membranes. In other words, there could be a link between the status of polyprotein processing in the nsp4-6 region and the membrane structures formed. This

idea is supported by observations made for an unrelated DMV-forming virus, HCV, for which it was recently shown that DMV formation became less efficient when the proteolytic cleavage of the NS4B/5A site in the viral polyprotein was accelerated (39).

The existence of different proteolytic processing intermediates containing nsp5 is well documented for arterivirus infection (84), although the role of the different precursors in DMV formation has not been studied so far. Unfortunately, the kinetics of polyprotein processing by M^{pro} in MERS-CoV and SARS-CoV are still largely unknown. M^{pro}'s enzymatic activity has mainly been assessed using recombinant nsp5 and peptide substrates *in vitro* (76, 177, 179, 194), but an analysis of the kinetics in a large(r) polyprotein setting is mostly lacking. Most information on the processing of the coronavirus nsp4-nsp10 region is derived from studies on other coronaviruses, such as MHV, IBV and HCoV-229E (the latter two being a gamma- and alphacoronavirus, respectively) (76, 198, 199). An in-depth analysis of the kinetics of polyprotein maturation during coronavirus infection, the identification of nsp6-containing processing intermediates, and the investigation of their possibly distinct roles in membrane remodeling could help to unravel the mechanisms underlying the formation of the coronavirus ROs.

Acknowledgements

Gijs Versteeg (Max F. Perutz Laboratories, Vienna, Austria), Michael Buchmeier (University of California, Irvine, USA), Ralf Bartenschlager (Heidelberg University, Heidelberg, Germany), and Ron Fouchier (Erasmus Medical Center, Rotterdam, the Netherlands) are cordially acknowledged for providing reagents. Anja de Jong (EM section, Leiden University Medical Center) is thanked for technical assistance, and LUMC colleagues Peter Bredenbeek and Alexander Gorbalenya are thanked for helpful discussions.

MATERIALS AND METHODS

Cells, viruses, and antibodies

HuH-7 cells (kindly provided by Dr. Ralf Bartenschlager; Heidelberg University) were grown in Dulbecco's modified Eagle's medium (DMEM; Lonza) supplemented with 8% (v/v) FCS (Bodinco), 2 mM L-glutamine (PAA Laboratories) and non-essential amino acids (PAA Laboratories). 293T cells (kindly provided by Virgin lab; Washington University School of Medicine in St. Louis) were cultured in DMEM with 10% (v/v) FCS. All cell culture media contained 100 U/ml penicillin and 100 µg/ml streptomycin. Infection of HuH-7 cells with MERS-CoV (EMC/2012 strain kindly provided by Ron Fouchier; Erasmus Medical Center, The Netherlands; (12, 173)) was performed as previously described (128).

Primary antibodies used were mouse α-HA (Clone HA.C5; Abcam), mouse α-β-actin (Clone AC-74; Sigma), mouse α-V5 (Clone 2F11F7; Thermo Fisher). A rabbit serum recognizing SARS-CoV-nsp3 that cross-reacts with MERS-CoV nsp3 has been previously described (106, 128). A polyclonal rabbit serum was used against a combination of two MERS-CoV nsp5 peptides; SGLVKMSHPSGDVEAC (amino acids 3248-3263 of pp1a) and CPADQLSDPNYDALLI (3291-3306) which was produced by Eurogentec.

Plasmid construction and transfection

Human codon-optimized coding sequences of MERS-CoV nsp3-6 were designed using GeneART™ and ordered from Thermo Fisher in four fragments and subsequently assembled in low-copy vector pACNR1180 (200) using conventional cloning. The precise parts of MERS-CoV pp1a used for polyprotein constructs are outlined in Table S1. The nsp4 construct included the 21 C-terminal aa of nsp3 to prevent the N-terminal hydrophobic region of nsp4 from acting as a signal sequence, which could result in improper membrane insertion. In all constructs with a C-terminal myc- or V5-tag, the C-terminal glutamine of the viral sequence was omitted to prevent the removal of the tag by M^{pro}. The SARS-CoV nsp3 gene (Frankfurt 1 strain, pp1a amino acids 819-2740) was synthesized by Bio Basic Inc. (Ontario Canada). Coding sequences were transferred to the pCAGGS expression vector (Addgene) for expression. pCAGGS-SARS-nsp4 was described previously (28). 293T cells were transfected using Lipofectamine 2000 (Thermo Fisher) according to the manufacturer's instructions. HuH-7 cells were transfected using a Nucleofector 2b device (Lonza) with Nucleofector Kit T (Lonza) in 6x106 cells and 12 µg of plasmid DNA per transfection. Co-transfections were carried out with equimolar amounts of plasmids.

Western blotting

Cells were lysed in 2x Laemmli sample buffer (50 mM Tris-HCl, pH 6.8; 20% (v/v) glycerol; 4% (w/v) sodium dodecyl sulfate (SDS); 20 mM dithiothreitol; 0.02 mg/ml bromophenol blue) and separated by electrophoresis on SDS-polyacrylamide gels. Proteins were transferred to polyvinylidene fluoride membranes (Amersham) using a Trans-Blot Turbo transfer system (Bio-Rad). Blots were blocked with 5% (w/v) ELK skimmed milk powder (Campina) in phosphate-buffered saline (PBS) supplemented with 0.05% (v/v) Tween-20. Secondary HRP-conjugated antibodies (DAKO) and ECL Plus Western blotting substrate (Thermo Fisher) were used to visualize protein signal.

Immunofluorescence microscopy

After electroporation, HuH-7 were seeded on coverslips and fixed 24 hours later with 3% (w/v) paraformaldehyde in PBS. Samples were permeabilized with 0.2% (v/v) Triton X-100 and incubated with antibodies, including fluorescent conjugates, diluted in 5% (w/v) bovine serum albumin (BSA) in PBS. Nuclei were stained with 1 µg/ml Hoechst 33258. After embedding with Prolong Gold (Thermo Fisher), samples were analyzed with a Leica TCS SP8 confocal laser scanning microscope, which was equipped with a 63x objective (NA 1.40; 1 Airy Unit) and a Leica HyD hybrid detector.

Metabolic labeling and immunoprecipitation

293T cells were metabolically labeled with 100 µCi/mL [^{35}S]methionine and [^{35}S]cysteine (EXPRE35S35S Protein Labeling Mix; Perkin-Elmer) from 4 hours post-transfection onwards. Cells were lysed at 18 hours post-transfection in 20 mM Tris-HCl (pH 7.6), 150 mM NaCl, 0.5% (w/v) deoxycholic acid, 1% (v/v) Nonidet P-40, and 0.1% (w/v) SDS. Lysates were diluted in immunoprecipitation (IP) buffer (20 mM Tris-HCl (pH 7.6), 150 mM NaCl, 5 mM EDTA, 0.1% (w/v) DOC, 0.5% (v/v) NP-40, and 0.5% (w/v) SDS) and incubated with

antibody overnight. Antibody-protein complexes were then pulled down using Protein A and Protein G sepharose beads (GE healthcare), which were first blocked with 2% (w/v) BSA in PBS, and incubated for several hours. After repeated washing of the beads with IP buffer, proteins were eluted by heating in 2x Laemmli sample buffer. After separation on large 10% polyacrylamide gels and gel drying, signal was visualized using an Imaging Screen-K (Bio-Rad) and a Typhoon 9410 scanner (GE Healthcare).

Electron microscopy

Transfected HuH-7 or 293T cells were fixed 24 hours post-transfection in 1,5% (w/v) glutaraldehyde in 0.10 M cacodylate buffer (pH 7.4) for 1 hour at room temperature. After washing in 0.14 M cacodylate buffer, samples were post-fixed and stained at 4°C with 1% (w/v) osmium tetroxide in 0.10 M cacodylate buffer for 1 hour. After washing with 0.14 M cacodylate and Milli-Q water, cells were scraped and stained with 1% (w/v) tannic acid in Milli-Q water on a 3D rotator for 1 hour at room temperature. Following washing with Milli-Q water, cells were spun down in heated 3% (w/v) agar in PBS and after solidification pellets were excised, cut into small blocks and dehydrated in increasing concentrations of ethanol. Samples were embedded in epoxy resin (LX-112; Ladd Research) and after polymerization 100-nm sections were placed on mesh-100 copper EM grids covered with a carbon-coated pioloform layer. Following post-staining with 7% (w/v) uranyl acetate and Reynolds lead citrate samples were analyzed on an FEI Tecnai 12 BioTwin equipped with an Eagle cooled slow-scan charge-coupled device (CCD) camera (FEI) and operated at 120 kV. Measurements of circular profiles from 2D-EM images were done with ImageJ software and Aperio Imagescope software (Leica). Circular profiles were measured over their longest and shortest axis and the geometric mean of those values was used as the diameter. 100 circular profiles were measured for each condition.

Electron tomography

Sections of 150 nm thickness were cut from the resin-embedded blocks of transfected HuH-7 or 293T cells prepared as described above. Prior to post-staining, colloidal gold particles of 10 nm were applied to both sides of the EM grid to serve later as fiducial markers for alignment. Tomography data was recorded on an Eagle CCD camera (FEI) in an FEI Tecnai 12 BioTwin (HuH-7 samples) or a Twin (293T samples) electron microscope operated at 120 kV, with the grids mounted on a 2040 Fischione tomography holder. Dual-axis tilt series of the regions of interest were collected using Xplore3D software (FEI) at magnifications that resulted in a pixel size of 1.7 nm (BioTwin data) or 1.4 nm (Twin data). The angular coverage for each single-axis tilt series was 130 degrees sampled in increments of 1 degree. Alignment of the tilt series and tomogram reconstruction by weighted backprojection were performed in IMOD (170).

SUPPLEMENTARY MATERIAL

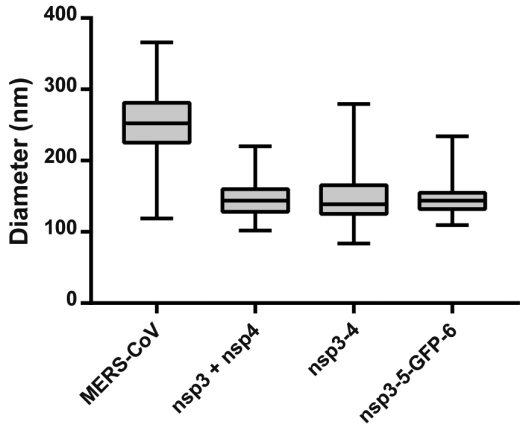

Supplementary fig. 1. Structures induced by MERS-CoV nsp3 and nsp4 are smaller than those observed during MERS-CoV infection. *The size of circular profiles was determined for MERS-CoV infected cells (10 h p.i.), for nsp3-4 expressing nsp3 and nsp4, the nsp3-4 self-cleaving precursor, and the nsp3-5-GFP-6 construct. 100 profiles were measured for each condition and plotted as a box and whiskers plot. The boxes show the 25th to 75th percentile and the whiskers the total range of the measurements.*

Construct	N-terminal tag	Polyprotein Start	Polyprotein End	C-terminal tag
nsp3-4	HA	854	3246	V5
nsp3	HA	854	2739	c-myc
nsp4	-	2720	3246	V5
nsp3-6	HA	854	3844	V5
nsp3-6-GFP[1]	HA	854	3850	GFP
nsp3-5-GFP	HA	854	3558	GFP
nsp3-5-GFP-6[2]	HA	854	3560	GFP
nsp5-6	-	3242	3844	V5

Table S1. Details of MERS-CoV expression constructs. *The parts of MERS-CoV pp1a used for the different expression constructs are listed in the table. Amino acid numbers are based on pp1a of MERS-CoV EMC/2012 strain. The coding sequence was human codon optimized unless otherwise indicated. (1) Amino acids 3561 – 3850 were not codon-optimized but the MERS-CoV sequence. (2) GFP was followed by MERS-CoV pp1a amino acids 3548-3844 fused to a V5-tag at the C-terminus.*

Supplementary movies

Tomographic reconstructions of areas showing membrane structures induced by coronavirus nsps. HuH-7 cells co-transfected with constructs expressing MERS-CoV nsp3 and nsp4 (Movie S3) or transfected with a construct expressing the self-cleaving nsp3-4 precursor (Movie S4) were analyzed by ET. The movies move along the Z-axis in consecutive virtual slices of 1.67 nm thickness. Five DMVs that are fully reconstructed in the tomogram are indicated with green dots. The distinctive feature that unambiguously identifies a vesicle in a tomogram is a circular profile that is largest at the vesicle's equator and decreases in diameter when moving up or down from that plane through successive tomographic slices until, if the vesicle is fully contained in the section, it disappears. Scale bars represent 500 nm.

293T cells co-transfected with SARS-CoV nsp3 and nsp4 constructs were also analyzed by ET. Two areas are shown, one with relatively more zippered-ER (Movie S5) and the other with more DMVs (Movie S6). The movies progress first in the Z-axis along consecutive slices (1.42 nm thick) and then loops back marking with green dots all the DMVs that were fully reconstructed within the tomogram (i.e. originally fully contained in the cell section). Scale bars represent 500 nm. The movies will be available with the online version of the article that has been accepted for publication in mBio (mBio 8(6) e01658-17).